August 2001 • NREL/SR-520-30811

Subcontractor Report

Photocharge Transport and Recombination Measurements in Amorphous Silicon Films and Solar Cells by Photoconductive Frequency Mixing

Annual Subcontract Report
20 April 1999 – 19 April 2000

R. Braunstein, A. Kattwinkel, and S.R. Sheng
University of California
Los Angeles, California

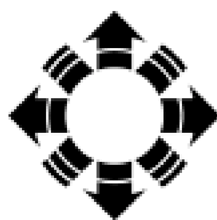

National Renewable Energy Laboratory

1617 Cole Boulevard
Golden, Colorado 80401-3393

NREL is a U.S. Department of Energy Laboratory
Operated by Midwest Research Institute • Battelle • Bechtel

Contract No. DE-AC36-99-GO10337

August 2001 • NREL/SR-520-30811

Photocharge Transport and Recombination Measurements in Amorphous Silicon Films and Solar Cells by Photoconductive Frequency Mixing

Annual Subcontract Report
20 April 1999 – 19 April 2000

R. Braunstein, A. Kattwinkel, and S.R. Sheng
University of California
Los Angeles, California

NREL Technical Monitor: B. von Roedern

Prepared under Subcontract No. XAK-8-17619-24

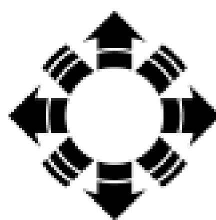

National Renewable Energy Laboratory

1617 Cole Boulevard
Golden, Colorado 80401-3393

NREL is a U.S. Department of Energy Laboratory
Operated by Midwest Research Institute • Battelle • Bechtel

Contract No. DE-AC36-99-GO10337

NOTICE

This report was prepared as an account of work sponsored by an agency of the United States government. Neither the United States government nor any agency thereof, nor any of their employees, makes any warranty, express or implied, or assumes any legal liability or responsibility for the accuracy, completeness, or usefulness of any information, apparatus, product, or process disclosed, or represents that its use would not infringe privately owned rights. Reference herein to any specific commercial product, process, or service by trade name, trademark, manufacturer, or otherwise does not necessarily constitute or imply its endorsement, recommendation, or favoring by the United States government or any agency thereof. The views and opinions of authors expressed herein do not necessarily state or reflect those of the United States government or any agency thereof.

Available electronically at http://www.doe.gov/bridge

Available for a processing fee to U.S. Department of Energy
and its contractors, in paper, from:

U.S. Department of Energy
Office of Scientific and Technical Information
P.O. Box 62
Oak Ridge, TN 37831-0062
phone: 865.576.8401
fax: 865.576.5728
email: reports@adonis.osti.gov

Available for sale to the public, in paper, from:

U.S. Department of Commerce
National Technical Information Service
5285 Port Royal Road
Springfield, VA 22161
phone: 800.553.6847
fax: 703.605.6900
email: orders@ntis.fedworld.gov
online ordering: http://www.ntis.gov/ordering.htm

Printed on paper containing at least 50% wastepaper, including 20% postconsumer waste

Preface

The National Amorphous Silicon research team consists of focused subteams to improve the individual component cells from which the multijunction devices are fabricated. The Mid-bandgap and Metastability subteam and the Low Bandgap subteam have the responsibility to develop appropriate materials for the respective layer of the triple junction solar cell. To this end, it is necessary to characterize the materials that are prepared for the appropriate layer to optimize the devices and to develop an understand of the conditions responsible for light-induced degradation so as to develop means to mitigate the degradation. Using the photomixing technique, UCLA was able to determine the mobility and lifetime separately of a number of semiconductor materials. We have established that different kinetics of degradation occur for mobility and lifetime. We have found that the drift mobility is electric field dependent and developed a model for the charge transport through long range potential fluctuations which enable a determination of the range and the depth of these fluctuations for material in the annealed and light soaked states. UCLA has continued to provide transport parameters for the mid-gap, metastability, and low-band teams. The materials studied were prepared by various deposition techniques.

In phase II of this program, we have investigated in detail the charge transport properties by photomixing of a-Si:H, μc-Si:H and a-SiGe:H alloy films prepared by the hot wire chemical vapor deposition (HWCVD) and the plasma enhanced chemical vapor deposition (PECVD) techniques, particularly under the conditions of the high deposition rate and the transition from amorphous to microcrystalline state. Photomixing experiments were initiated on comparison of intrinsic film properties and device performance, and on study of the impact of the changed contact geometry on the results of our photomixing measurements. We also attempted to employ the photomixing technique to measure the drift mobility of TCO. Following our previous measurements of the transport parameters under hydrostatic pressure, we initiated the hydrostatic pressure dependence of small angle X-ray scattering measurements to try to find out the origin of the inelastic effect. Time resolved photo- and thermoelectric effects (TTE) were used to simultaneously determine the thermal diffusivity, carrier lifetime, carrier mobility, and trap level density in crystalline and amorphous Si (a-Si:H) and Si/Ge (a-Si/Ge:H) samples.

Table of Contents

Page

Preface ……………………………………………………………………….…….…..…...i

Table of Contents …………………………………………………….………..………...ii

List of Figures ………………………………………………….……………..…......iii

List of Tables …………………………………………………………….…..…...…...v

Introduction …………………………………………………….……………….…….1

Results and Analysis …………………………………………….…………….……2

1. The “uninterrupted growth/annealing” method ………………….……………...2

   Photomixing measurements on samples supplied by Guanglin Kong………...…3

2. Initial experiments on single film samples with coplanar and perpendicular contact geometry………………………………...………...……..9

3. Comparison of intrinsic film properties and device performance………………......12

4. Charge transport properties in the transition from amorphous to microcrystalline silicon produced by MVSystems…………………………….…18

   The first set of samples……………………………………………………18

   The second set of samples……………..…………………………...………19

5. Hydrostatic pressure dependence of charged transport and small angle X-ray scattering measurements……………...……………………….…..20

6. High deposition rate preparation of a-Si:H by HWCVD……………….………...….…21

   Measurements of transport properties of high deposition rate HWCVD a-Si:H films in the annealed state…………………………...……..22

   Light-induced decay measurements of transport properties of high deposition rate HWCVD a-Si:H films…………………………….………26

7. Photoconductive Frequency Mixing Measurements on TCO……………...……..30

References…………………………...…...………………………………….…31

Publications……………………………..………..…………………………..…..32

List of Figures

Figure 1. Samples G202 and G179, dilution ratio is kept constant at 1:5.

Figure 2. Samples G203 and G204, dilution ratio is kept constant at 1:5.

Figure 3. Samples I70426 and I80929.

Figure 4. Samples P60715I with flat and rough surface; These are prepared by employing the "uninterrupted growing/annealing" technique.

Figure 5. Sample schematics for measurements in two field directions.

Figure 6. DC and AC currents with perpendicular contact geometry(Film thickness 5244Å).

Figure 7. Field dependent mixing power for both configurations. For the TCO–a-Si:H–Al sample, the zero-field point was shifted according to the mixing power minimum at V = -0.5V (Fig. 6).

Figure 8. Light-induced changes in photoconductivity, mobility, and lifetime of film R8796 (H_2 diluted, using RF).

Figure 9. Light-induced changes in photoconductivity, mobility, and lifetime of film R8794 (H_2 diluted, using VHF).

Figure 10. Photo current for nip-devices in the annealed state.

Figure 11. Square root of mixing signal for nip-devices in the annealed state.

Figure 12. Normalized decay of the dc photocurrent in short circuit condition, and the back-bias mixing signal in nip device R8791.

Figure 13. Normalized decay of the dc photocurrent in short circuit condition and the back-bias mixing signal in nip device R8792.

Figure 14. Normalized decay of the dc photocurrent in short circuit condition and the back-bias mixing signal in nip device R8793.

Figure 15. Light-induced changes of photoconductivity, mobility, and lifetime for sample MVS 968.

Figure 16. The photoconductivity as a function of deposition rate.

Figure 17. The drift mobility as a function of deposition rate.

Figure 18. The lifetime as a function of deposition rate.

Figure 19. Field dependence of the drift mobility (a) and lifetime (b) for sample L183.

Figure 20. The depth (a) and range (b) of the long range potential fluctuations as a function of deposition rate.

Figure 21. The relative change in the charged defects as a function of deposition rate.

Figure 22. The hydrogen content as a function of deposition rate.

Figure 23. Normalized photoconductivity, drift mobility and lifetime for high deposition rate HWCVD a-Si:H samples as a function of illumination.

Figure 24. The light-induced changes in the photoconductivity, drift mobility and lifetime as a function of deposition rate.

Figure 25. The light-induced changes in the depth and range of potential fluctuations as a function of deposition rate.

Figure 26. The light-induced relative change in the charged defect density as a function of deposition rate.

List of Tables

Table 1. Deposition conditions of samples supplied by Guanglin Kong

Table 2. Long-range potential fluctuations (Guanglin Kong)

Table 3. Growth conditions of the films and the respective i-layers in the n-i-p structures

Table 4. Long-range potential fluctuations (Uni-Solar)

Table 5. Sample data as provided by MVSystems

Table 6. Growth conditions and properties of high deposition rate HWCVD Samples

Introduction

In the present phase of the program, the transport parameters of a number of amorphous semiconductors prepared by a number of techniques were determined by the photoconductive frequency mixing technique. This technique enabled us to determine the drift mobility, μ_d, and the photomixing lifetime, τ. The technique is based on the idea of heterodyne detection for photoconductors. When two similarly polarized monochromatic optical beams of slightly different frequencies are incident upon a photoconductor, the photocurrent produced, when a dc bias applied, will contain components resulting from the square of the sum of the incident electric fields. Consequently, a photocurrent composed of a dc and a microwave current due to the beat frequency of the incident fields will be produced; these two currents allow a separate determination of the drift mobility and the photomixing lifetime of the photogenerated carriers [1-6]. The photomixing technique can be related to the modulated photocurrent technique[7],this technique is performed at low frequencies. In the present work, the longitudinal modes of a He-Ne laser were employed to generate a beat frequency of 252 MHz; all the measurements were performed at this frequency for the data indicated in the accompanying figures. Employing this technique, the following topics were explored whose results will be presented in the following sections:

1. Photomixing Measurements on a-Si:H samples prepared by the "uninterrupted growth/annealing" method supplied by Guanglin Kong.
2. Initial experiments on single film samples with coplanar and perpendicular contact geometry.
3. Comparison of intrinsic film properties and device performance.
4. Charge transport properties in the transition from amorphous to microcrystalline silicon produced by MVSystems
5. Hydrostatic Pressure Dependence of Charged Transport and Small Angle X-ray Scattering Measurements.
6. High Deposition Rate Preparation of a-Si:H by HWCVD: Measurements of transport properties in both the annealed and light-soaked states.
7. Photoconductive Frequency Mixing Measurements on TCO.

Publications

1- Determination of the gap state density differences in hydrogenated amorphous silicon and Si/Ge.

2- Electronic properties of hydrogenated amorphous silicon-germanium alloys and long-range potential fluctuations.

1. The “uninterrupted growth/annealing” method

During the last period a series of a-Si single film samples supplied by Guanglin Kong[1] was measured by means of the Photoconductive Frequency Mixing method. The series consists of four samples with varied deposition temperature (G179 – G204), two samples which were prepared for the investigation of light-induced structural changes, and two more samples prepared by means of the “uninterrupted growth/annealing” PECVD method which was developed by the Kong-group.

In contrast to the “Chemical Annealing” or layer-by-layer deposition where growth and H^+ annealing alternate, the hydrogen treatment happens during the deposition process. This approach which essentially amounts to hydrogen dilution as has been studied for years by, e.g., Tsu [8]. As also suggested by Tsu, the hydrogen plasma is kept at a level near the threshold to the formation of microcrystalline silicon. At this level, the etching effect of hydrogen during the growth process results in a more dense and stable Si network without the formation of larger microcrystalline regions. This leads to amorphous films with improved stability yet without the typical drawbacks of mixed or μc-Si films, i.e. lower optical response due to partly indirect transition, and lower mobility due to grain boundaries.

A slight boron compensation is believed to shift the Fermi level down towards the midgap which results in a higher photosensitivity as well as a higher electron mobility. CPM measurements on appropriately compensated a-Si samples also suggest a lowered subgap absorption which might be due to a passivation of native donor-like impurities through the formation donor-acceptor pairs, compensation of dangling bonds and release of local strain in the Si network.

According to [9] and [10],appropriate hydrogen dilution results in amorphous silicon films with light-induced decay of the photocurrent of about one half order of magnitude with saturation tendency after 10^4 seconds of illumination. With additional boron compensation, the samples show essentially stable photoconductivity properties. In comparison, an a-Si:H standard sample showed a photocurrent decay of about one order of magnitude. With samples where both hydrogen dilution and boron compensation were applied, even an *increase* of the photocurrent was found in some samples [9] which is explained in terms of an additional light-induced effect which involves a bond-switching from fourfold to threefold B configurations forming neutral acceptor dangling bond pairs. These, in turn, lower the B doping efficiency and therefore, in the case of slight B

[1] Institute of Semiconductors, Chinese Academy of Sciences, Beijing, China

compensation, result in a shift of E_f towards E_c and accordingly an increase of the electron mobility.

Photomixing Measurements on samples supplied by Guanglin Kong

The sample properties are given in Table I.

Table 1. *Deposition conditions*

Sample ID	$SiH_4:H_2$	ingredient	$T_{substr.}$ (^oC)	T_{dep} (hrs)	Thickness (μm)	Deposition Rate (Å/s)
I 70426	1:1		360	4.5	1.5	0.93
I 80929	1:3		300	3.5	3	2.40
P 60715 I	1:12	0.2% $B_2H_6(10^{-4})$	225	3.0	0.89	0.82
P 60717 II	1:12	2% $B_2H_6(10^{-4})$	225	2.6	0.79	0.84
G 179	1:5		350	1.5	1.25	2.31
G 202	1:5		400	4.0	1.7	1.18
G 203	1:5		300	5.0	3.2	1.78
G204	1:5		200	3.0	2.2	2.04

As shown in Table 1, a series of four samples, G179 - G204, is prepared with the substrate temperature being varied at constant dilution ratio. The respective light-induced decay curves are shown in figures 1 and 2 beginning with the highest substrate temperature. For all samples, the mobility after three hours of illumination lies somewhere between 50% and 60% of the initial value. The lifetime decay, however, seems to scale with the deposition temperature, i.e. the lower the deposition temperature the lower the final lifetime with respect to the initial value. Also the initial photomixing mobility is clearly higher for films deposited with higher T_s. For the photoconductivity this means that for lower deposition temperatures ($T_s < 350^oC$) both the initial value (due to the lower initial mobility) and the decay rate (due to the higher decay of the lifetime) turn out to be rather poor as compared to samples with $T_s \geq 350^oC$. It seems that given a moderate dilution ratio the network reconstruction during growth requires more activation through the substrate temperature than, e.g. in the case of Hot-Wire CVD. From this series it is clear that the best sample is also the most expensive one in terms of substrate temperature and deposition rate.

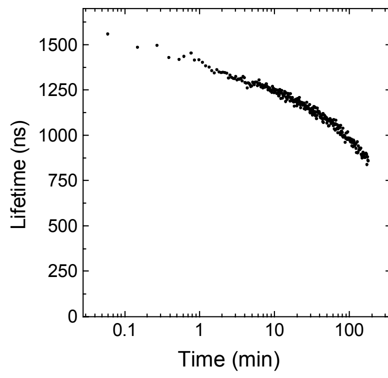

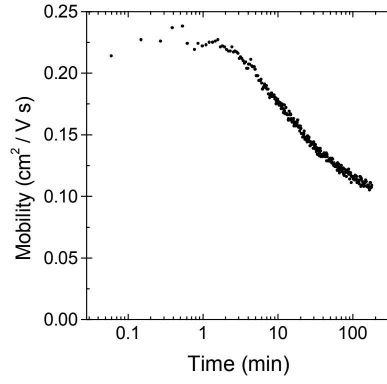

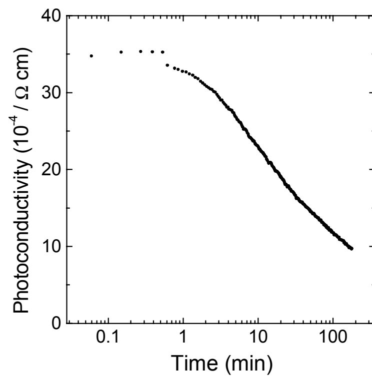

Sample G202

$T_{depos.}$ = 400 ^{o}C

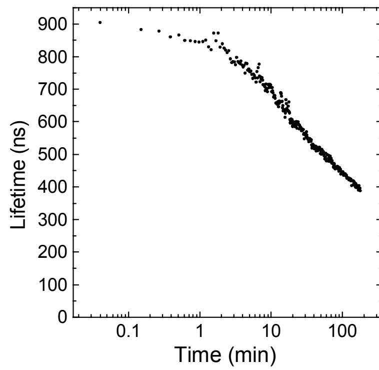

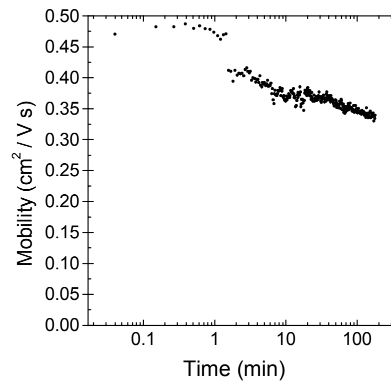

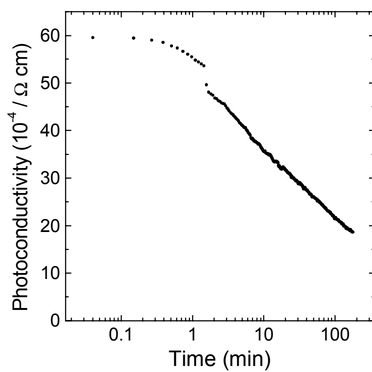

Sample G179

$T_{depos.}$ = 350 ^{o}C

Figure 1. *Samples G202 and G179, dilution ratio is kept constant at 1:5*

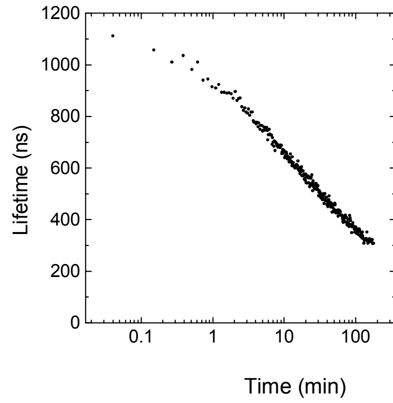

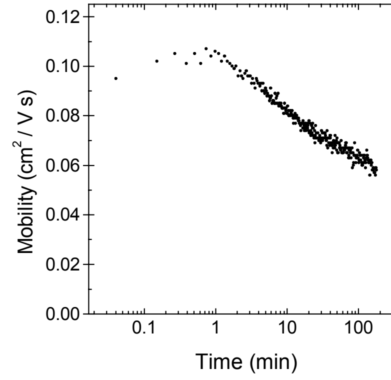

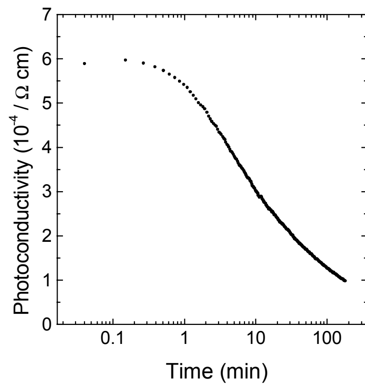

Sample G203

$T_{depos.}$ = 300 ^{o}C

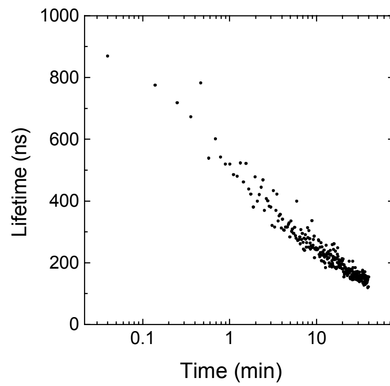

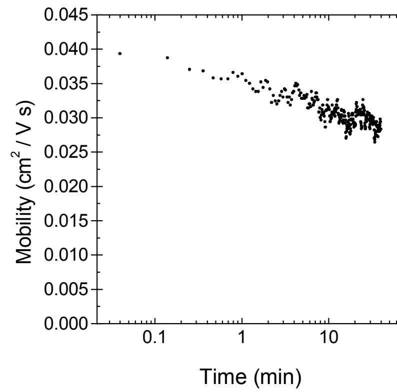

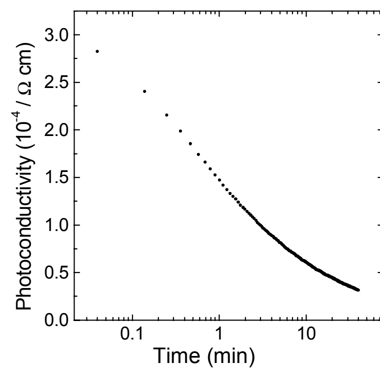

Sample G204

$T_{depos.}$ = 200 ^{o}C

Figure 2. *Samples G203 and G204, dilution ratio is kept constant at 1:5*

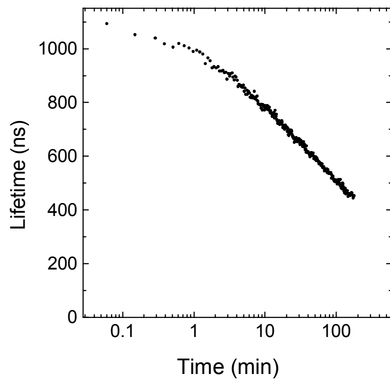

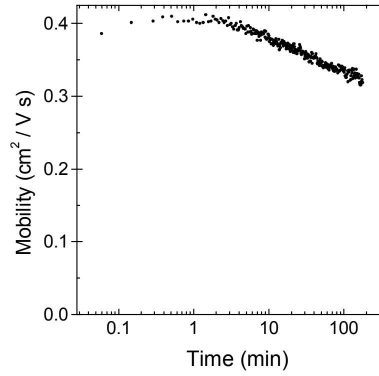

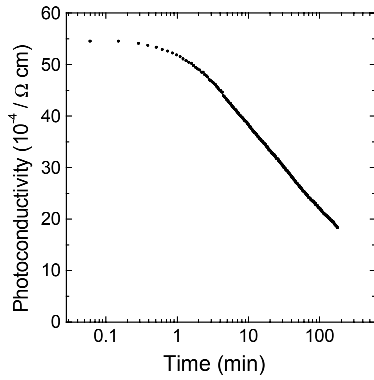

Sample I70426

$T_{depos.}$ = 360 °C
$SiH_4 : H_2$ = 1:1

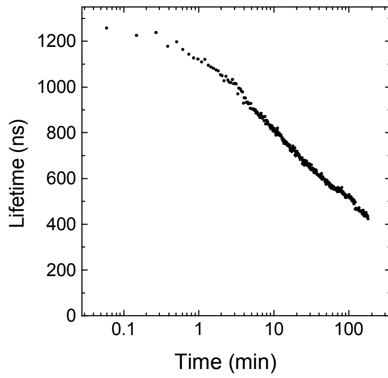

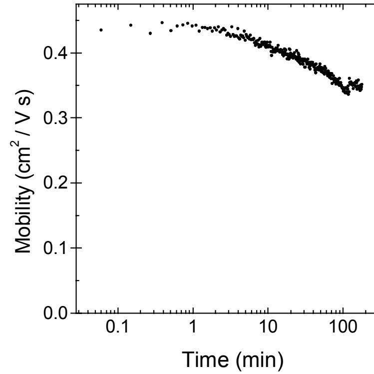

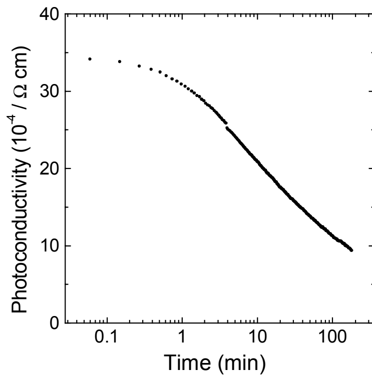

Sample I80929

$T_{depos.}$ = 300 °C
$SiH_4 : H_2$ = 1:3

Figure 3. *Samples I70426 and I80929.*

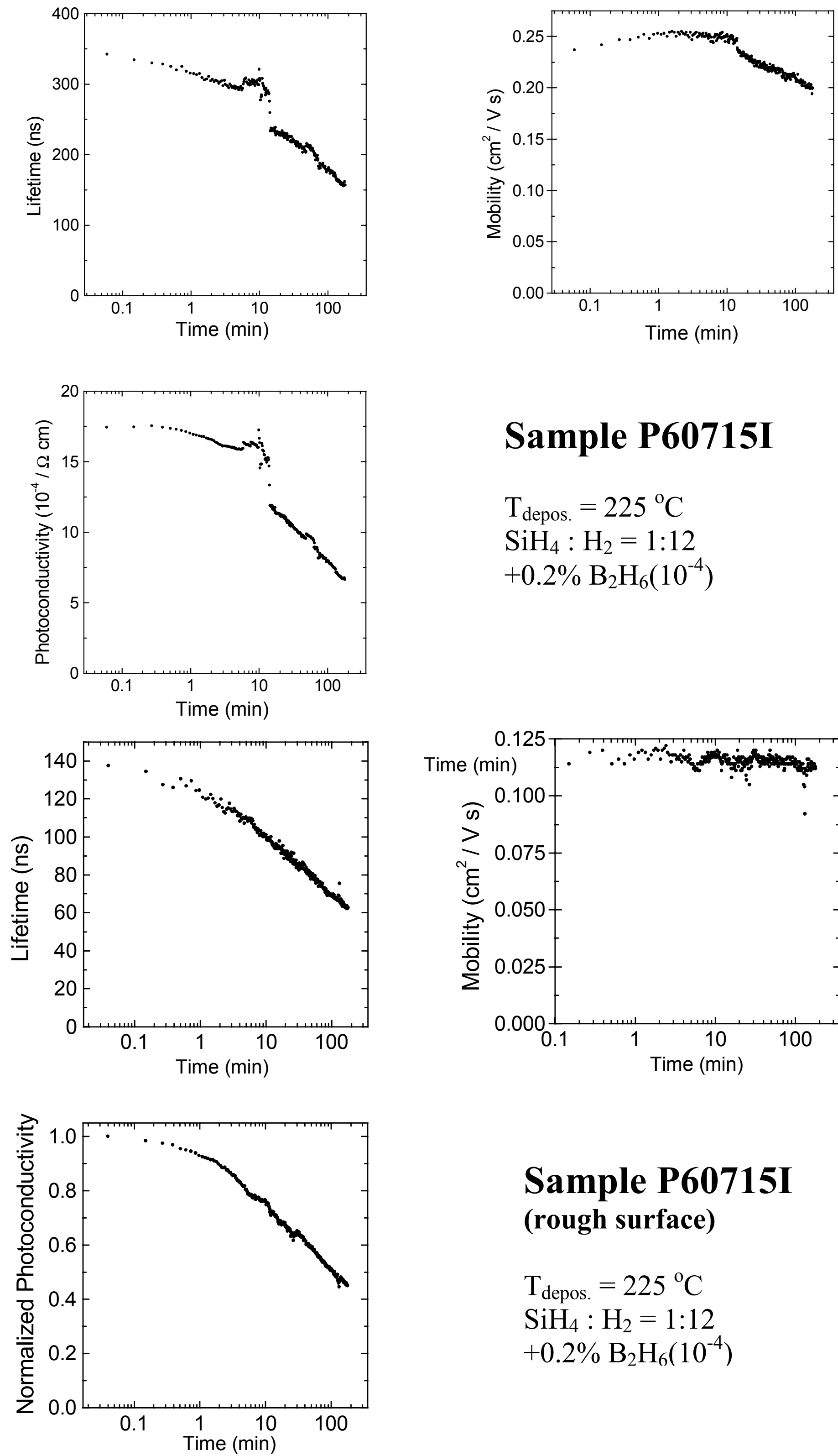

Figure 4. *Samples P60715I with flat and rough surface; These are prepared by employing the "uninterrupted growing/annealing" technique.*

From figure 3, we can see that samples I70426 and I80929 again suggest that the substrate temperature has a large impact on the film stability. The sample with lower hydrogen dilution ratio but higher substrate temperature shows better stability at a higher performance level. The deposition rate of I80929, on the other hand, is about three times that of I70426. This means that other parameters not specified by the Kong group may have been changed, too. However, the thicknesses of I70426 and I80929 were just estimated from the deposition period.

Finally, Figure 4 shows our results for the two samples prepared by "uninterrupted growth/annealing" PECVD, P60715I and P60717II. Actually, we had two 'P60715I' samples available, one with a flat and one textured surface. Both P60715I samples show a decay of all transport quantities in the range of 20% (mobility) through about 50% - 60% (lifetime, photoconductivity). However, a first slight increase in mobility is observable (P60715I – flat surface) but after about 15 min the mobility begins to decrease, too. In comparison to the samples with mere dilution and from our results of the light-induced decay, we cannot detect any noticeable impact of boron doping on transport for the present samples other than what is mentioned above, but samples are more stable.

Unfortunately, we were unable to detect any reasonable mixing signal on the P60717II. This is particularly disappointing since this would have been the only sample that we have access to independent data for [9].

Table 2 below summarizes the Long-range potential fluctuation data we acquired for the whole series. The values for LRPF range and depth reflect the good stability of the mobility in most samples, particularly I70426 and I80929.

Table 2. *Long range potential fluctuations*

Sample ID	H-Dilution	Substrate Temperature	Range (nm)	Range (nm)	Depth (eV)
I 70426	1:1	360	Annealed	83.3	0.10
			Light-soaked	83.3	0.11
I80929	1:3	300	Annealed	89.0	0.10
			Light-soaked	88.7	0.11
P60715I	1:12 $+B_2H_6$	225	Annealed	30.1	0.11
			Light-soaked	30.1	0.12
P60715I (rough s.)	1:12 $+B_2H_6$	225	Annealed	39.0	0.13
			Light-soaked	38.0	0.13
G179	1:5	350	Annealed	19.1	0.13
			Light-soaked	16.3	0.14
G202	1:5	400	Annealed	40.8	0.09
			Light-soaked	46.4	0.13
G203	1:5	300	Annealed	24.2	0.12
			Light-soaked	25.8	0.15
G204	1:5	200	Annealed	*Weak mixing signal / Low mobility*	
			Light-soaked		

2. Initial experiments on single film samples with coplanar and perpendicular contact geometry

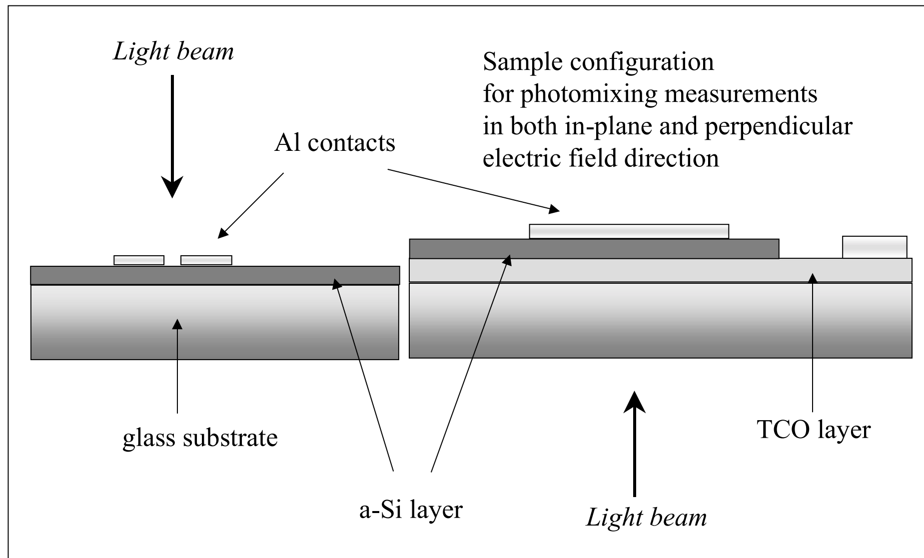

Figure 5. *Sample schematics for measurements in two field directions*

It has been noted that the electronic transport properties of plain films do not *directly* scale with the actual performance of solar cells built with those films as i-layers. Many complications such as non-uniform electric field, interface effects, etc. result in a dc-photocurrent which is highly convoluted and therefore no measure for the i-layer properties alone. The i-layer transport dependency of the photomixing signal, in particular, is obscured by the non-uniform electric field profile and the contact geometry related capacitance which acts as a parallel complex resistance muting the mixing signal. In an effort to separate these contributions we have initiated first measurements on single a-Si:H films with both coplanar and sandwich contact configuration.

As described in Figure 5, Brent Nelson (NREL) has prepared a sample for measurements in both cross-layer and in-plane electric field direction so that we have the chance to study the impact of the changed contact geometry on the results of our photomixing measurements. Two substrates, one plain glass and one TCO-coated, were evaporated with an intrinsic a-Si:H layer in the same run. The layer thickness is 0.524 microns (L148). Coplanar Al contacts were evaporated in coplanar configuration (glass substrate) and sandwich configuration (TCO-coated glass substrate).

Figure 6 shows our preliminary results for both the ac and dc signals. The sample shows pronounced non-ohmic behavior which can be due to the TCO—a-Si interface, the aluminum contacts or both.

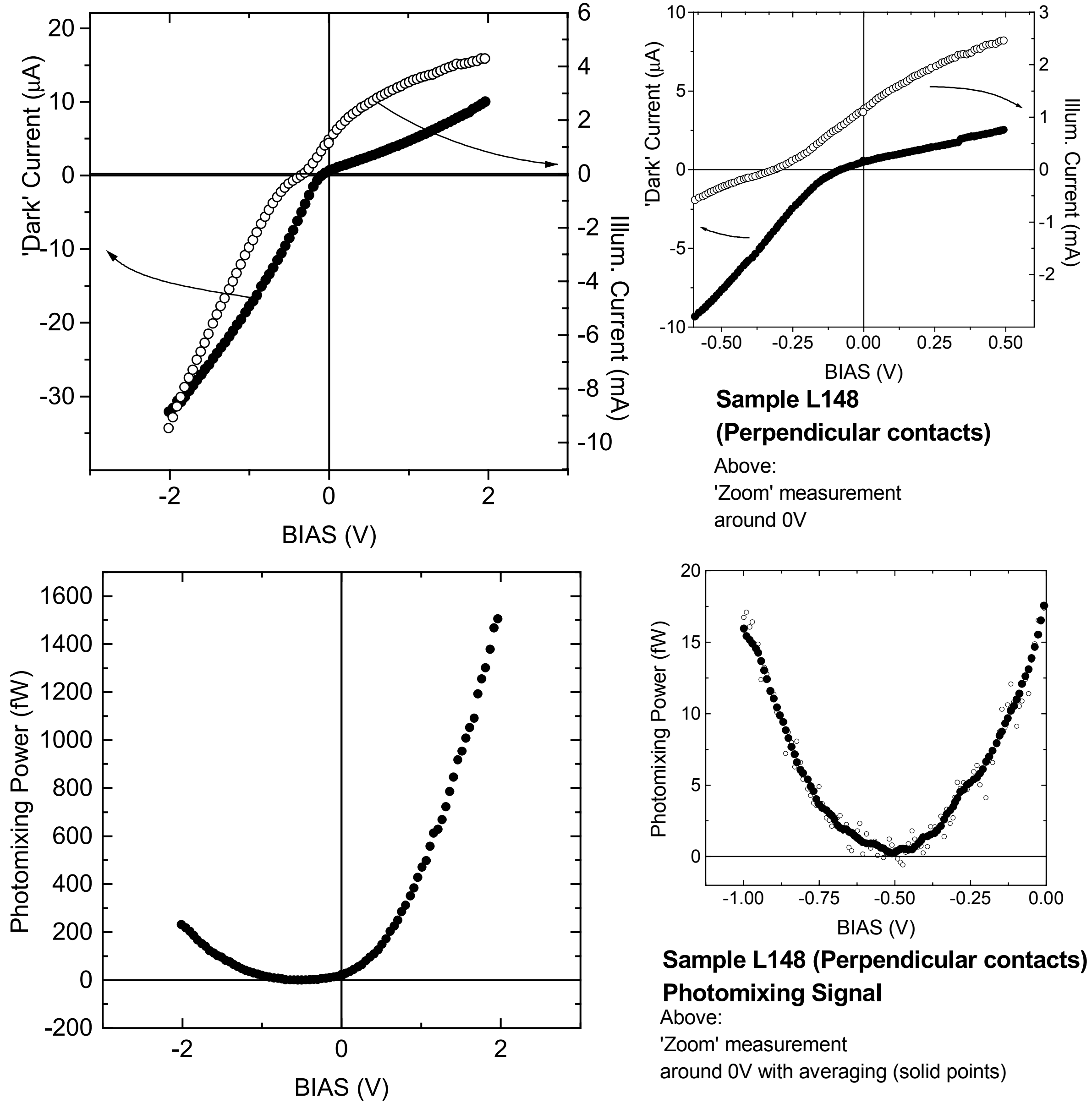

Figure 6. *DC and AC currents with perpendicular contact geometry (Film thickness 5244Å)*

While, according to B. Nelson and Qi Wang (NREL), it is very difficult to obtain ohmic contacts between TCO and intrinsic silicon layers, it seems possible to reduce the

accompanying effects (field profile distortion etc.) by increasing the layer thickness (which of course is limited by the light absorption profile to around 2µm) and choosing contact materials according to their work function.

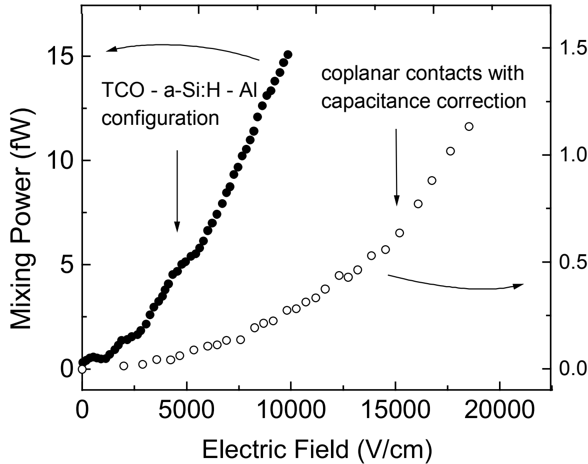

Figure 7. *Field dependent mixing power for both configurations. For the TCO–a-Si:H–Al sample, the zero-field point was shifted according to the mixing power minimum at V = -0.5V (Fig. 6)*

However, while the dc-curves suggest at least two non-ohmic contributions, we only find one distinct minimum of the mixing curve which indicates a zero-field condition within the intrinsic layer at an external BIAS of –0.5V.

Figure 7 shows a comparison between the mixing power obtained from the perpendicular contact configuration (solid points) and the sample with coplanar contacts.

For the sake of comparability, we estimated the power losses due to the inherent capacitance of the sample as 1.2nF (contact diameter = 2.5mm, film thickness = 0.54µm, dielectric constant for a-Si (GHz region) = 13.7). Using these assumptions the sample capacitance is 1.2 nF and accordingly, at a frequency of 252MHz, the complex resistance parallel to the photocurrent source is about 100 times lower than the setup impedance. With according corrections applied, it turns out that the mixing signal of the sample with coplanar contacts are much lower than in the transverse electric field case. Moreover, in the case of transverse field direction, we find a rather parabolic field dependence of the mixing power (Best seen in Fig. 6, small graph). Both indicates that with the electric field in transverse direction most charge carriers contributing to the current are swept out. Measurements on different samples with the above mentioned improvements will be carried out in order to show whether there is any significant impact of the i-layer preparation on the photomixing results.

3. Comparison of intrinsic film properties and device performance

During the last period a set of three intrinsic amorphous Si – film samples and related devices was investigated. The samples were made by S. Guha's group using the PECVD technique at United Solar. The n-i-p structures were prepared on stainless steel and ITO-coated. The intrinsic layers were grown according to the same recipe that was used for the respective films.

The idea is to investigate the relation between

- the initial a-Si:H film transport properties and the initial performance of the device
- the decay behavior of both film and related device.

Table 3 gives a summary of the sample preparation as provided by the Uni-Solar group.

Table 3. *Growth conditions of the films and the respective i-layers in the n-i-p structures*

Sample ID, film	Sample ID, device	Growth conditions
R8795	R8791	SiH_4 with no diluition, using RF
R8796	R8792	SiH_4 with H_2 dilution, using RF
R8794	R8793	SiH_4 with H_2 dilution, using VHF

Figures 8 and 9 show data taken from the intrinsic a-Si:H films R8796 and R8794. Both were produced with hydrogen diluted SiH_4. Unfortunately, we were not able to detect any photocurrent with sample R8795 which was produced without dilution. However, data could be obtained for all nip structures. The illumination intensity of one sun of the HeNe line was employed.

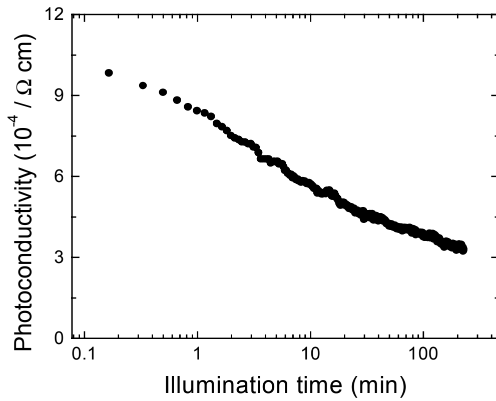

Figure 8.

Light-induced changes in photoconductivity, mobility, and lifetime of film R8796 (H_2 diluted, using RF)

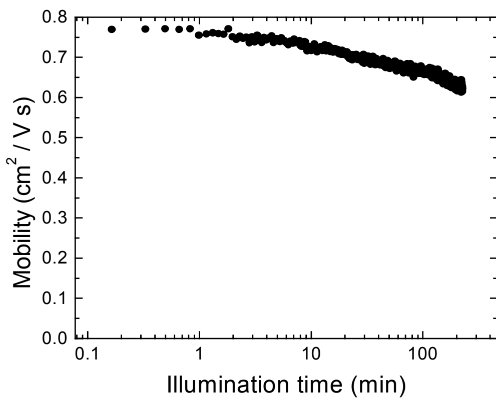

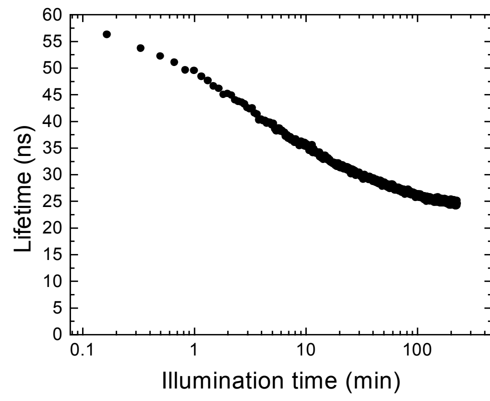

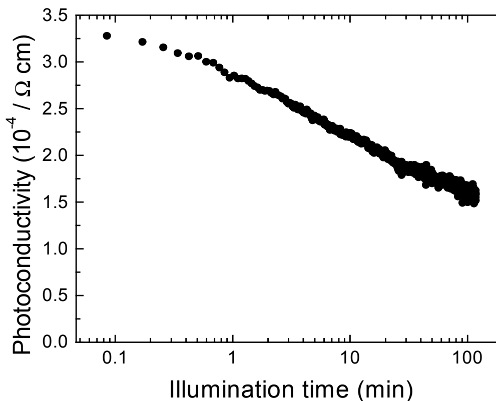

Figure 9.

Light-induced changes in photoconductivity, mobility, and lifetime of film R8794 (H_2 diluted, using VHF)

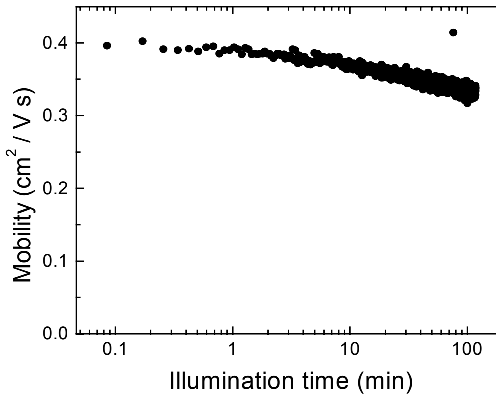

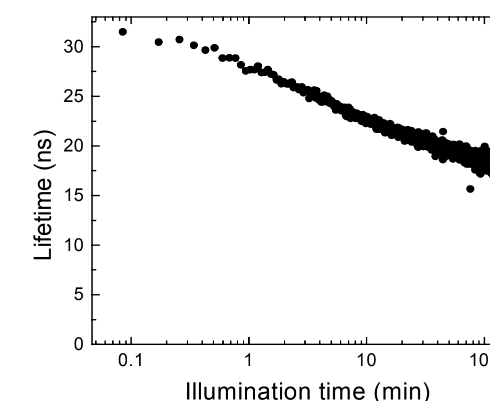

The difference between the films R8796 and R8794 is the plasma excitation frequency as can be seen in Table 3. The VHFCVD technique allows for an increase of the deposition rate at an almost linear function of the frequency to 5-10 times the deposition rate in the case of RF frequencies. Also, a reduced deposition temperature is possible, both of which is relevant in device applications. The film quality can still be high due to a decrease of the silicon-ion energy while the ion-flux is high. The transport parameters, however, are mainly dependent on other growth parameters which have to be reoptimized as one changes from RF to VHF.

In the case of the present two film samples we find for R8796 (RF excitation) an almost double as high a mobility as for R8794 (VHF excitation) in the annealed state. Also, the lifetime ratio between R8794 and R8796 is in the same range. From this we can clearly conclude that the transport properties of the RF – film is superior. As far as the decay is concerned, we find that for both samples the decrease of the lifetime is dominant which is also reflected in the results for the Long-Range Potential Fluctuation range and depth before and after light-soaking. These quantities are summarized in Table 4. It can be seen that neither range nor depth change much which shows that the density of charged defects stays more or less constant.

Table 4. *Long-range potential fluctuations*

Sample	State	LRPF range (nm)	LRPF depth (eV)
R8796	annealed	34.6	0.07
	light-soaked	34.5	0.08
R8794	annealed	39.8	0.09
	light-soaked	36.2	0.09

After 180 minutes of illumination, the decay of the photoconductivity of the RF film is a little higher in the case of the RF sample than for the VHF film. Since in a wide range H_2 dilution both improves both opto-electronic properties and stability of amorphous silicon films, it is interesting to see how the device behavior changes with respect to dilution and increase of frequency.

Figure 10 shows the initial I/V-curves for all nip structures. Again, the nip device made with an intrinsic film using RF (R8792) shows higher initial short circuit current than R8793 (VHF). The structure with the intrinsic layer made without dilution shows the lowest initial values. Figure 11 shows the square root of the mixing power for each sample which is linear to the high-frequency part of the photocurrent. It can be seen that only with back-biasing to –1.5V the photomixing signals differ noticeably. As already discussed in the 98-99 annual report, the main difficulty of mixing measurements on devices is the non-uniform profile of the defect distribution and the electric field. Therefore, interface effects might play a more dominant role for forward-biasing than the actual intrinsic film properties.

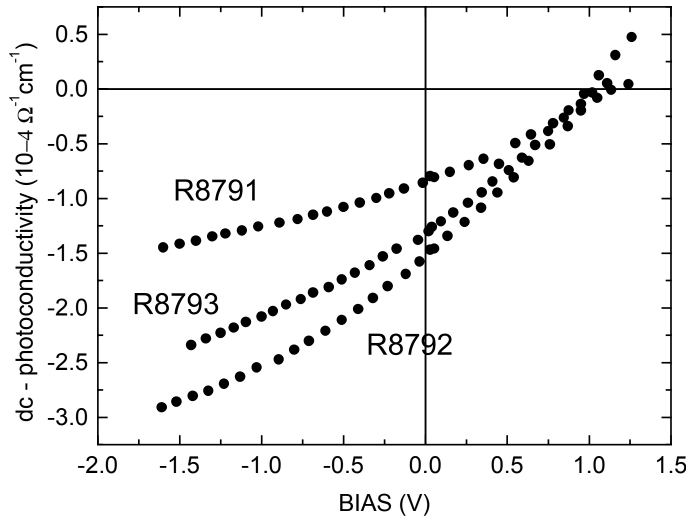

Figure 10.
Photo current for nip-devices in the annealed state.

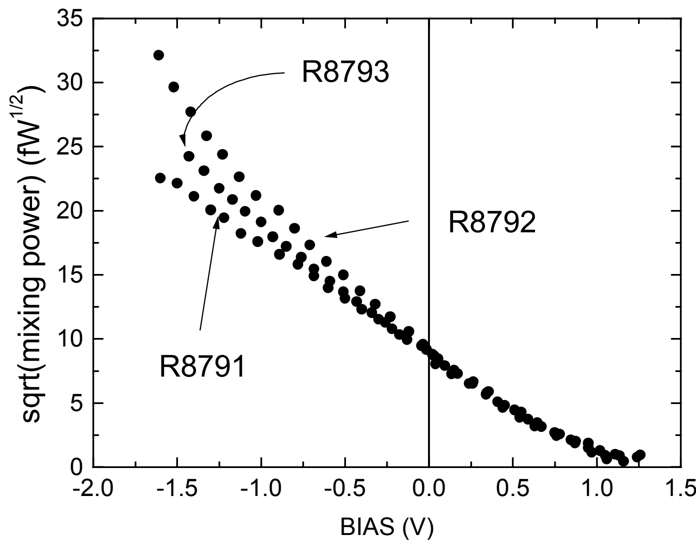

Figure 11.
Square root of mixing signal for nip-devices in the annealed state.

Figures 12, 13, and 14 finally give an overview of the light-induced decay measurements on the nip devices. While for sample R8793 (VHF) the back-bias photomixing signal seems to almost mimic the dc – short circuit current, we find the decay of the ac signal to be greater than the dc current for R8792 (RF) and the reverse case for R8791 (undiluted). Assuming that both illumination intensity (about 20 mW laser power) and back-biasing is sufficient in order to neutralize charged defect states near the interfaces, the present results would suggest that the decay of the intrinsic film in R8792 contributes less to the over-all decay of the solar cell than in the case of R8793 which would be consistent with the slightly smaller decay of the mobility of the R8796 film (which is incorporated in

R8792) than for R8794 even though the over-all decay of the photoconductivity is actually higher for R8796.

In summary this would mean that the decay of I_{sc} of the solar cells seems to scale with the initial performance of the respective single films. It certainly would have been more informative if we had been able to also acquire decay data on sample R8791 but in any case the experiments showed that

- the *initial* cell and film performances for the RF and VHF samples are consistent
- it is not clear whether the light-induced decay of the nip structures scale with the related films.
- There is a scaling between the properties of the film and ac- and dc- measurements on devices.

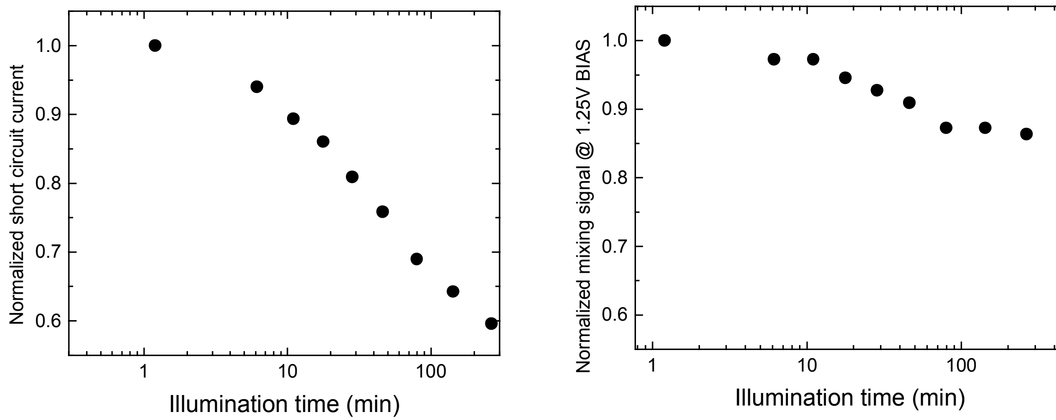

Figure 12. *Normalized decay of the dc photocurrent in short circuit condition and the back-bias mixing signal in nip device R8791*

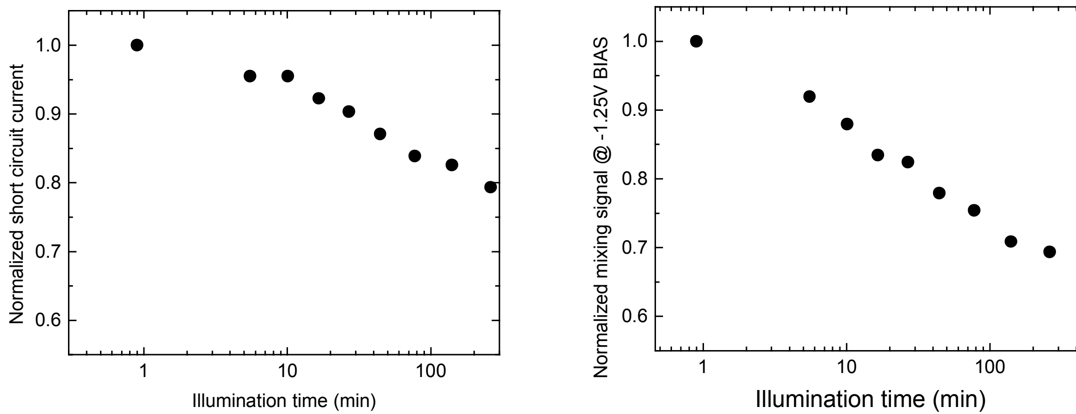

Figure 13. *Normalized decay of the dc photocurrent in short circuit condition and the back-bias mixing signal in nip device R8792*

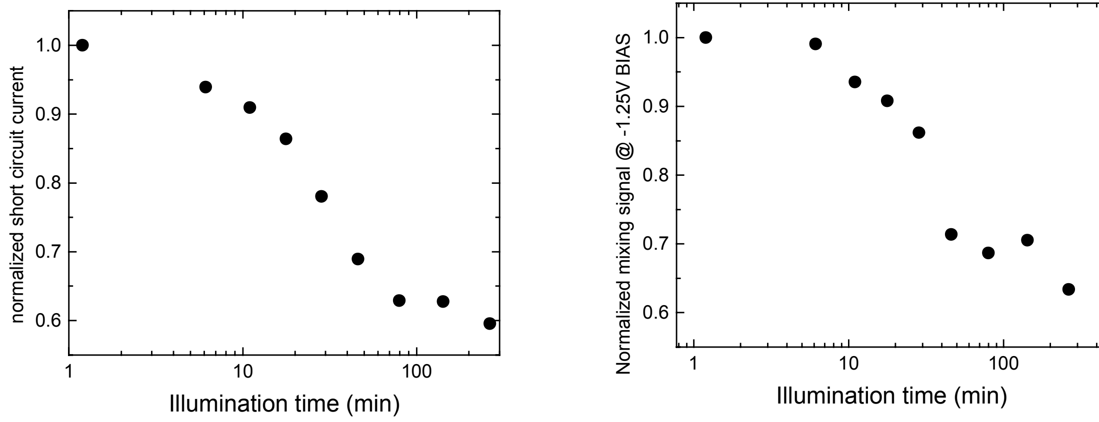

Figure 14. *Normalized decay of the dc photocurrent in short circuit condition and the back-bias mixing signal in nip device R8793*

4. Charge transport properties in the transition from amorphous to microcrystalline silicon produced at MVSystems

The first set of samples

The series discussed here was provided by MVSystems. It consists of eight samples starting in the completely amorphous regime (MVS 968) in numerical order through to microcrystallinity (MVS 975 and MVS 1003). In Table 5 the corresponding sample data is listed.

Table 5. ***Sample data as provided by MVSystems***

Sample ID	**Filament Temperature**	**H_2 dilution**	**Dark cond. $(\Omega cm)^{-1}$**	**Light cond. $(\Omega cm)^{-1}$**	**Thickness (Å)**
968	Low	0	$1.0*10^{-10}$	$3.1*10^{-5}$	6,000
969	High	0	$1.5*10^{-7}$	$1.8*10^{-7}$	70,000
970	High	20	$8.5*10^{-7}$	$2.5*10^{-6}$	9,200
971	High	50	$9.5*10^{-10}$	$1.3*10^{-8}$	19,000
972	High	80	$3.0*10^{-8}$	$6.8*10^{-8}$	16,000
973	High	90	$4.3*10^{-7}$	$4.7*10^{-7}$	9,000
975	High	95	$2.2*10^{-6}$	$2.4*10^{-6}$	7,300
1003	High	93	$3.1*10^{-5}$	$3.2*10^{-5}$	22,500

Figure 15 shows the decay data of the amorphous sample 968. The electric field dependent mobility for this sample yields the range (R) and depth (D) of the Long-Range Potential Fluctuations:

Annealed State: R = 40.4nm, D = 0.14eV
Light-soaked state: R = 38.7nm, D = 0.16eV

Unfortunately, we were unable to obtain data on most of the other samples as the photoresponse of these is generally low and therefore not suitable for our mixing method. Only on MVS 970 we could detect a mixing signal at an electric field of 22kVcm^{-1} for which we obtained a photomixing mobility μ_D = 0.035cm^2/Vs and a photomixing lifetime of around 60ns.

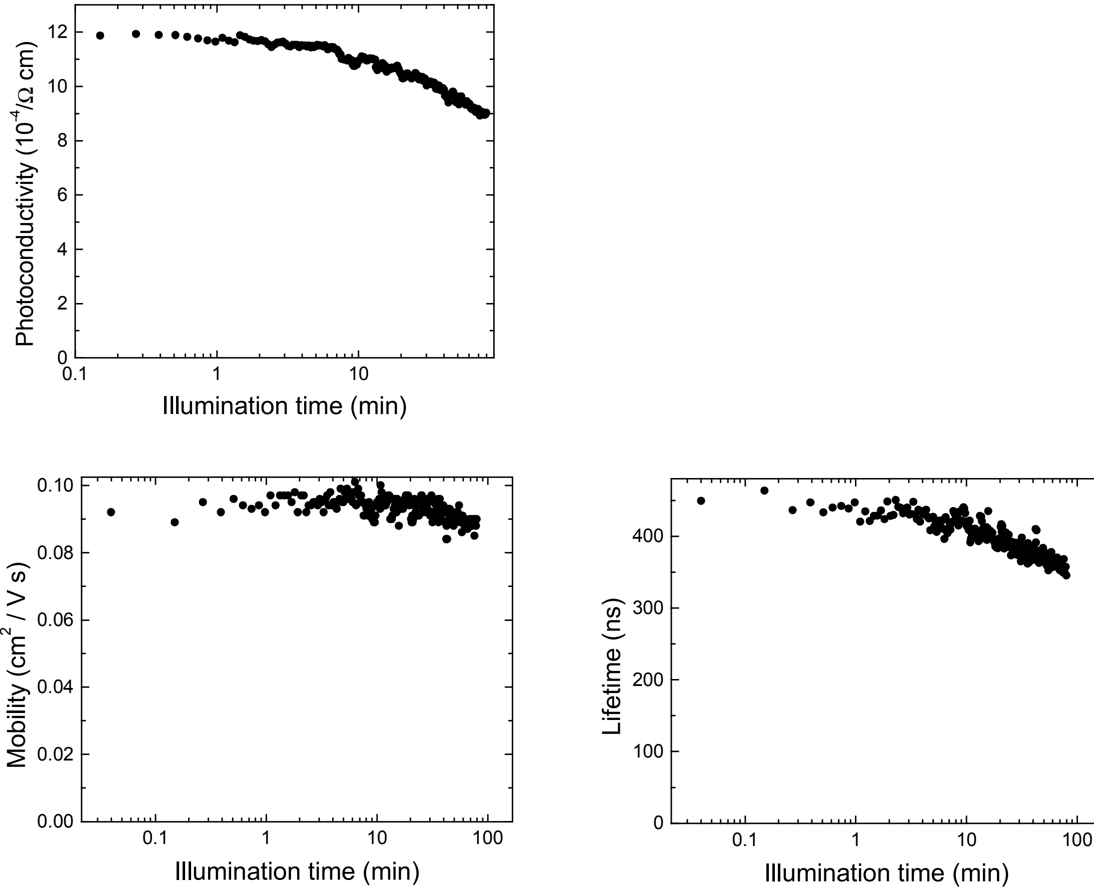

Figure 15. *Light-induced changes of photoconductivity, mobility, and lifetime for sample MVS 968*

The second set of samples

We have received another set of HWCVD H-diluted intrinsic microcrystalline silicon films from MVSystems for photomixing transport measurements. These samples were made on glass substrates with different filament-substrate distance, substrate temperature and H-dilution. Some of the samples were made on c-Si substrates. We have performed preliminary photomixing measurements on these samples in the annealed state, and obtained some good results, which were found to be somewhat similar to those we reported previously on NREL HWCVD samples in the transition from amorphous to microcrystalline silicon. While, more samples near the transition regime are required from MVSystems in order to investigate more in detail the charge transport properties in the transition materials.

Light soaking measurements and FTIR measurements are being initiated on these samples.

5. Hydrostatic Pressure Dependence of Charged Transport and Small Angle X-ray Scattering Measurements

We had previously reported on a series of measurements on the charge transport properties of amorphous silicon determined by photomixing as a function of hydrostatic pressure. It was found that under a given pressure the photoconductivity and mobility decreased while the lifetime increased. However, when the pressure was released a partial recovery of the photoconductivity and mobility was observed but not to the values obtained at the initial zero pressure. These results indicate there are two effects of hydrostatic pressure; one an *elastic* effect where the mobility decreases under pressure but is restorable when the pressure is released and an *inelastic* effect where the mobility stays decreased due to the introduction of charge scattering centers. It was conjectured that a permanent collapse of the voids in a-Si:H may be responsible for the inelastic component.

To this end samples were supplied by Don Williams which we subjected to hydrostatic pressure. Subsequently, the SAXS measurements were performed by Don Williams at the Colorado School of Mines. The samples consisted of one low temperature preparation with a relatively high void fraction (about 2 vol%) and one a high substrate temperature with a very low void fraction ($\leq$ 0.02 vol%). The SAXS data showed no evidence for residual microvoid collapse. Therfore, the origin of the inelastic component is still unknown. Other changes to be considered are bond angles and bond lengths.

6. High Deposition Rate Preparation of a-Si:H by HWCVD

The deployment of solar cells for large scale power generation is contingent not only upon the production of photovoltaic devices of stable high efficiency but for industrial production, high deposition rate is desirable to improve the throughput for a given machine. It has been suggested that with increasing deposition rates, higher silane related radicals, short-lifetime radicals, increased ion-bombardment energies, and hence more resultant microvoids and defects, are potential causes for deterioration of the performance and stability of hydrogenated amorphous silicon (a-Si:H) films. Various techniques to improve the deposition rate have been attempted: with plasma enhanced chemical vapor deposition (PECVD) which usually yields material with poor initial performance and poor stability when deposition rates are increased, which has been correlates with the increased density of microvoids [11]. A correlation between the gas phase species in the silane plasma and the properties of a-Si:H films deposited by PECVD has indicated that the higher-order silane species contribute to the cause of light-induced degradation in the film quality at high deposition rates [12]. The growth rate of these a-Si:H films ranged from 2 Å/s to 20 Å/s.

At present, it is generally believed that the performance of a-Si:H will deteriorate monotonically with increasing deposition rates, but the high deposition rates achieved by PECVD are relatively low, less than 20 Å/s. We have performed photoconductive frequency mixing measurements on much higher deposition rate HWCVD a-Si:H samples provided by Brent Nelson of NREL, and found some interesting results. The charge transport properties of the samples do not change monotonically with increasing deposition rates.

Brent Nelson has employed the HWCVD technique to prepare a-Si:H films grown with deposition rates ranging from 32 to 191 Å/s. He achieved the high deposition rates by making the following changes to one of his HWCVD reactors.

Deposition Parameter	**Standard Config.**	**High Dep. Rate Config.**
Number of filaments	1	2
Filament to substrate spacing	5 cm	3.2 cm
Silane flow rate	20-50 sccm	50-100 sccm
Deposition Pressure	10-20 mTorr	20-120 m Torr

Brent Nelson has informed us: "The deposition rate is a complicated function of the pressure, silane flow, and filament current. These are the three main parameters we change to alter the deposition rate. The increase in silane flow is necessary to accommodate the increased silane depletion due to multiple filaments. The increased pressure is necessary." We were supplied with the following samples whose preparation parameters are indicated in the Table 6.

Table 6 *Growth conditions and properties of high deposition rate HWCVD samples.*

Sample ID	Temp. (°C)	Press. (mTorr)	F(SiH_4) (sccm)	I(fil.) (A)	Thk. (Å)	Rate (Å/s)	Cond. Rate	H(IR) (at.%)
L079	295	20	20	30	6644	31.64	1.29×10^4	4.51
L077	295	70	20	30	8530	47.39	1.17×10^4	4.81
L110	285	19	75	30	10514	58.41	8.60×10^4	9.50
L139	315	50	50	29	8144	67.87	1.15×10^5	7.10
L169	318	50	50	30	9235	76.96	1.02×10^5	6.50
L104	350	50	50	30	10179	84.83	1.11×10^5	7.50
L183	348	70	75	30	11000	109.78	5.72×10^4	5.60
L178	317	70	75	30	11381	113.58	2.63×10^4	6.50
L182	348	70	75	30	11502	114.79	8.63×10^4	4.90
L190	326	50	75	30	9318	132.74	5.64×10^4	6.70
L196	325	75	75	30	8538	142.30	2.30×10^4	5.80
L094	385	90	75	30	13701	152.23	2.37×10^4	6.79
L194	325	70	100	30	10662	177.70	2.64×10^2	5.00
L087	295	120	75	30	22900	190.83	5.73	—

We have characterized these samples in both the annealed and light-soaked states utilizing the photoconductive frequency mixing technique enabling us to determine the drift mobility, lifetime and from the electric field dependence of these quantities, we have been able to determine the range and the depth of the long range potential fluctuations and from the latter two quantities we were able to determine the relative differences in the charge centers which exist in the samples.

Measurements of transport properties of high deposition rate HWCVD a-Si:H films in the annealed state

The photoconductivity as a function of deposition rate is shown in Figure 16. It is seen that in the deposition range from 30 Å/s to ~150 Å/s, the photoconductivity hovers at levels of 10^{-4} (S/cm) except that in the neighborhood of the deposition rate of 70 Å/s, the photoconductivity peaks in the neighborhood of 10^{-2} (S/cm), two orders of magnitude increase above the average ! Above the deposition rate of ~150 Å/s, the photoconductivity starts to plummet to 10^{-8} (S/cm) !

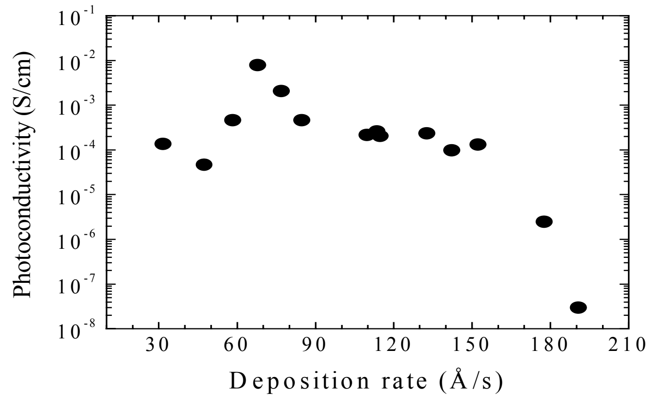

Figure 16. *The photoconductivity as a function of deposition rate*

By measuring the photomixing signal at 250 Mhz in conjunction with the dc photoconductivity, we determined the drift mobility and the lifetime. Figure 17 shows the drift mobility as a function of deposition rate. Where it is seen that the drift mobility peaks in the neighborhood of 70 Å/s where the photoconductivity peaks. However, it should be noted that the drift mobility varies by integer values, while the photoconductivity varies by orders of magnitude. These differences can be accounted for by the fact that the lifetime as a function of deposition rate varies by orders of magnitude as can be seen in Figure 18.

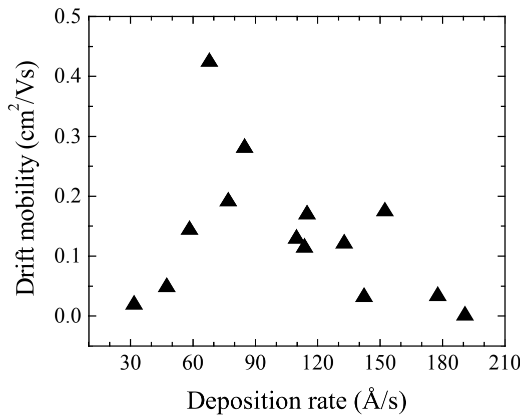

Figure 17. *The drift mobility as a function of deposition rate*

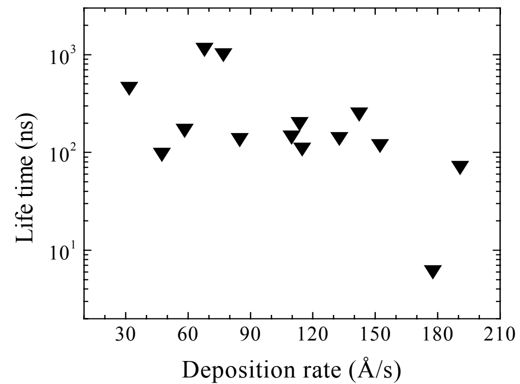

Figure 18. *The lifetime as a function of deposition rate*

Figure 19 shows a typical electric field dependence of the drift mobility (a) and lifetime (b). From this type of data, we have calculated the range and depth of the long range potential fluctuations which are shown in Figure 20. It should be observed that minimal depth of potential occurs in the region where the drift mobility and photoconductivity peaks as is to be expected.

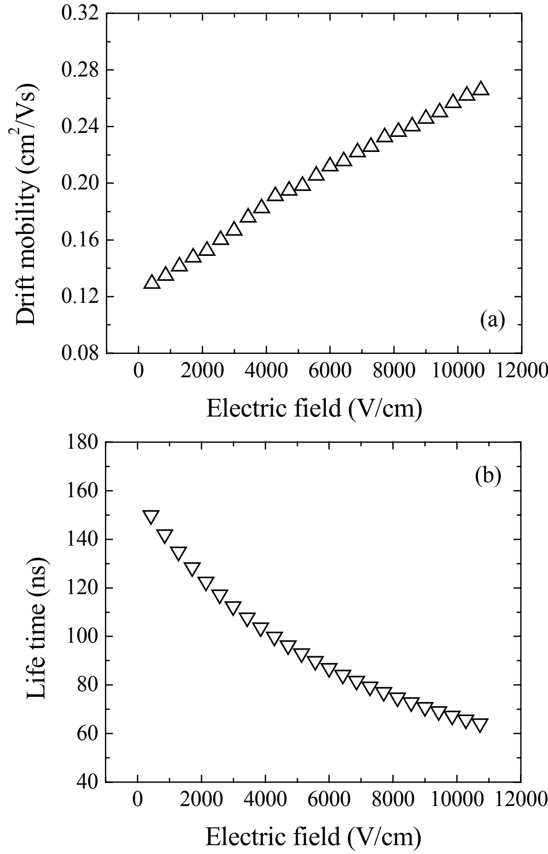

Figure 19. *Field dependence of the drift mobility (a) and lifetime (b) for sample L183.*

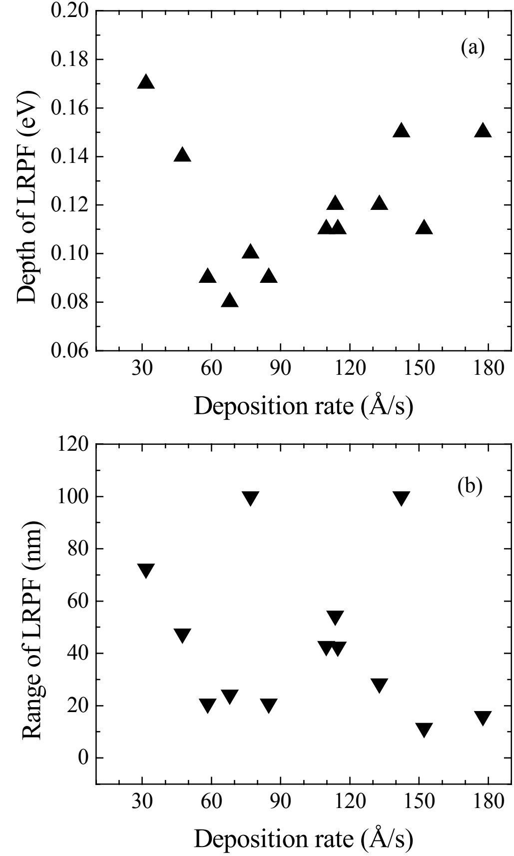

Figure 20. *The depth (a) and range (b) of the long range potential fluctuations as a function of deposition rate.*

It can be shown that the density of charge defects (n) is given by:

$$n \propto V_P^{\,2} / L \qquad (1)$$

Where V_P and L represent the depth and range of the long range potential fluctuations, respectively.

Figure 21 shows the relative change in the charged defects as a function of deposition rate. It can be seen that the charged defect density remains constant up to the deposition rate of ~150 Å/s, but above, it increases considerably.

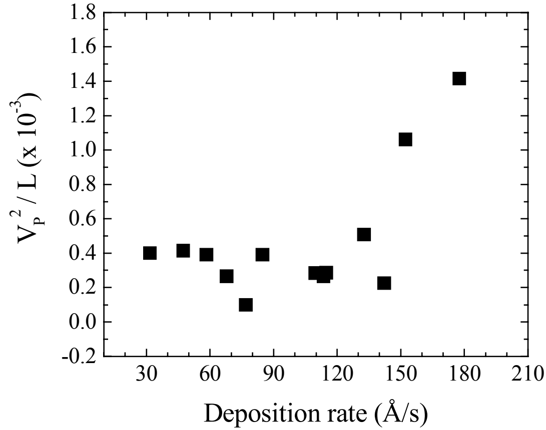

Figure 21. *The relative change in the charged defects as a function of deposition rate*

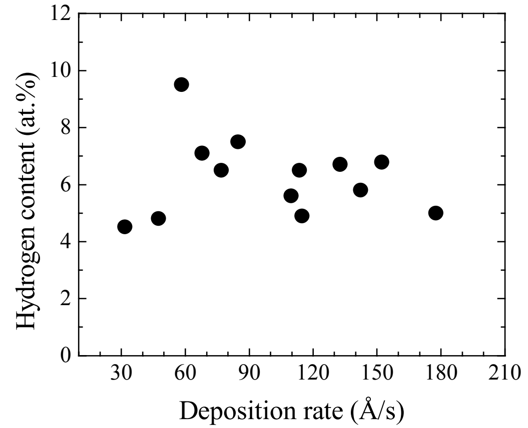

Figure 22. *The hydrogen content as a function of deposition rate*

It is of great interest to ascertain what are the chemical or structural properties of the films that vary as a function the deposition rate. The hydrogen content of the samples as a function of deposition rate is shown in Figure 22. It is interesting to note that maximal hydrogen content appears to occur in the region where the drift mobility and photoconductivity peaks, while elsewhere, the hydrogen content is comparable, about 6 at.%. It is clear that it is necessary to look for other film properties that are responsible for variation of charge transport properties as a function of deposition rate. It would be of interest to determine the microvoid and higher order silane content by performing SAXS and IR measurements in the Si-H stretching mode region.

Brent Nelson has provided us some preliminary IR results. There is no increase in dihydride bonding with increasing deposition rate. Table II shows qualitative results of SiH_2 shoulder at 2009 cm^{-1} from the IR spectra. We found that both dark-conductivity and photoconductivity of the samples with detectable SiH_2 shoulder are smaller than those of other samples without detectable SiH_2 shoulder, indicating poorer performance. In addition, we anticipate David Cohen's DLCS measurements of defect density are available.

Light-induced decay measurements of transport properties of high deposition rate HWCVD a-Si:H films

Figure 23 shows the normalized photoconductivity (a), drift mobility (b) and lifetime (c), respectively, for three typical high deposition rate HWCVD a-Si:H samples as a function of illumination time.

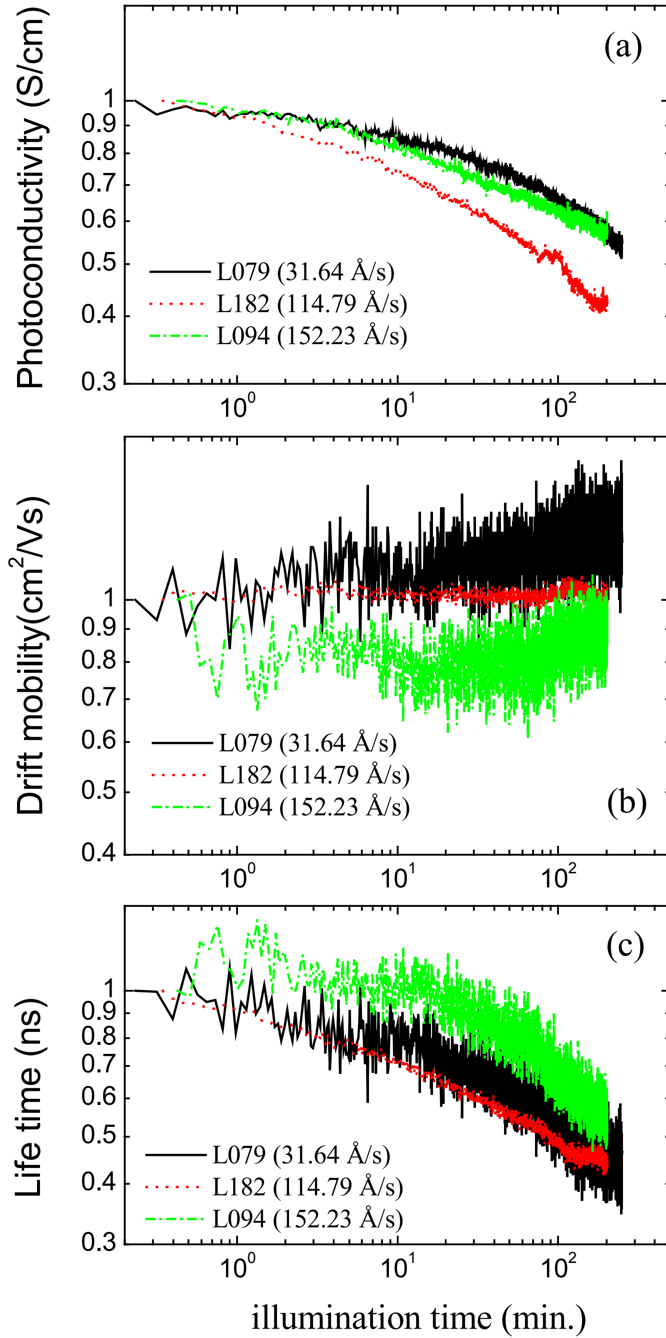

Figure 23. *Normalized photoconductivity, drift mobility and lifetime for high deposition rate HWCVD a-Si:H samples as a function of illumination.*

It is seen that with light-soaking, the photoconductivity for all the samples decreases, which is demonstrated to be attributed to considerable decreases in the lifetime. It is interesting to note that the drift mobility changes very small, even a little increase upon light-soaking!

In order to investigate more in detail the influence of illumination on the transport properties of the samples as a function of deposition rate, we performed systematical measurements on all samples whose deposition rates range from 32 to 191 Å/s. The photoconductivity, drift mobility and lifetime as a function of deposition rate in both the annealed and the light-induced states are shown in Figure 24 (a), (b) and (c), respectively. It can be seen that light-soaking reduces the photoconductivity and the lifetime, as observed before, while surprisingly increases the mobility for all the samples. Furthermore, the deposition rate dependence of these transport parameters in the light-soaked state is similar to that in the annealed state. Since the mobility varies only by integer values, while the lifetime varies by orders of magnitude, the light-induced decrease in the photoconductivity is mainly due to the decrease in the lifetime.

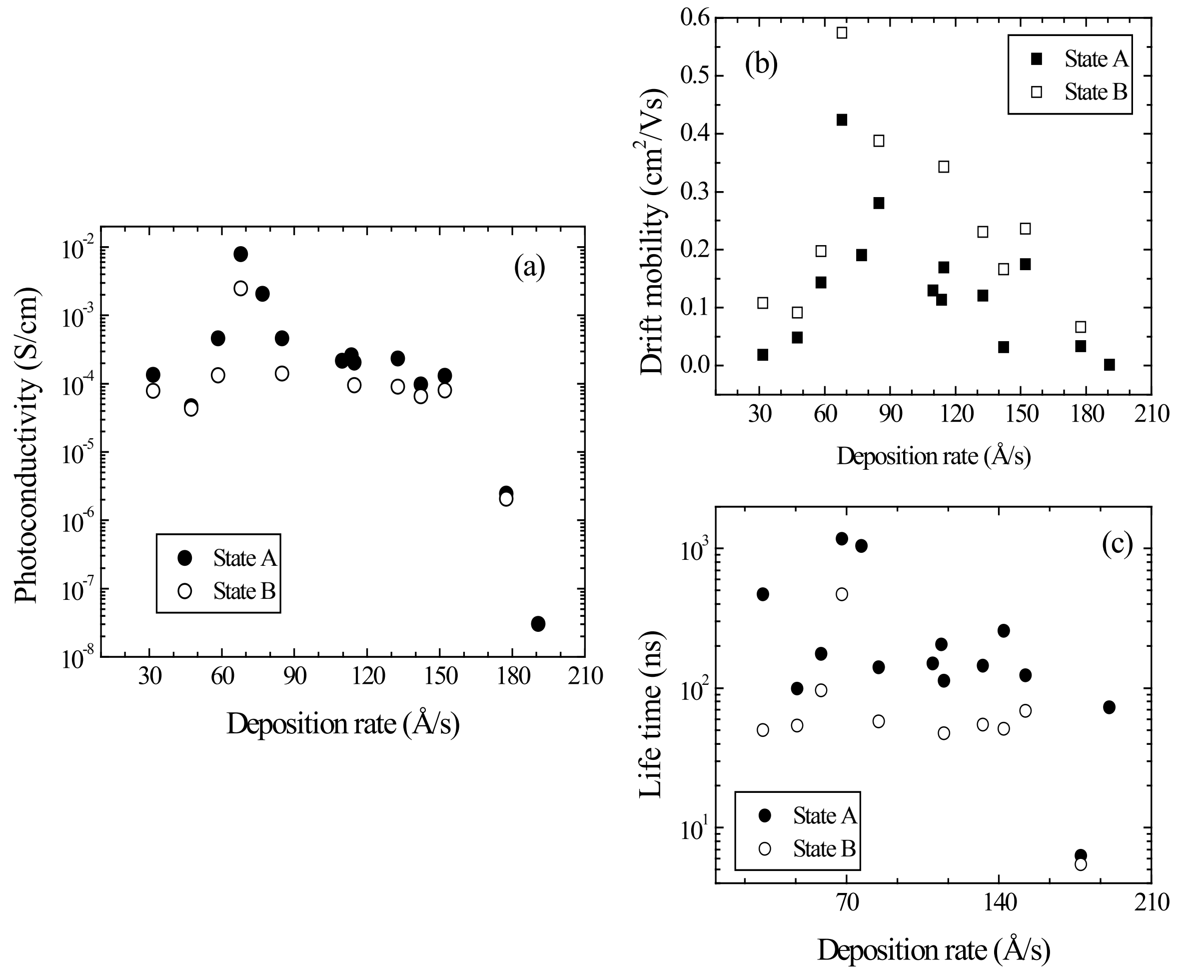

Figure 24. *The light-induced changes in the photoconductivity, drift mobility and lifetime as a function of deposition rate.*

From the electric field dependence of the drift mobility and lifetime, we have calculated the depth and range of the long-range potential fluctuations. Figure 25 shows the effect of light-soaking on the depth (a) and range (b) of potential fluctuations as a function of deposition rate.

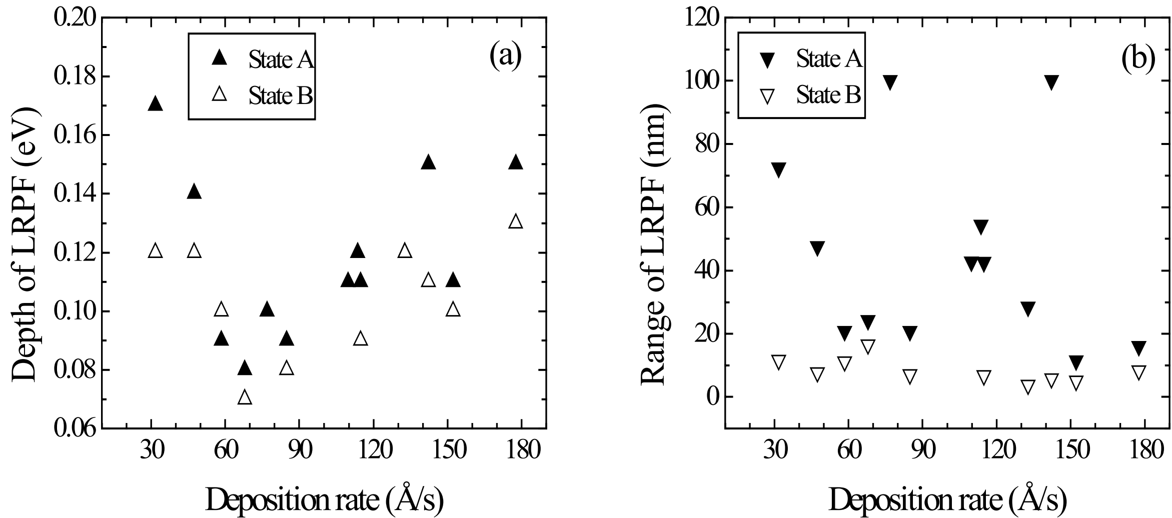

Figure 25. *The light-induced changes in the depth and range of potential fluctuations as a function of deposition rate*

Figure 26 shows the light-induced relative change in the density of charged defects as a function of deposition rate. We see that the charged defect density increases upon light-soaking for all deposition rates. It is interesting to note that there appears to be the minimum light-induced increase at the intermediate deposition rates where the photoconductivity, drift mobility and lifetime peak. In addition, it is generally expected that due to the increase in the density of charged defects during the light-soaking process, the depth of the potential fluctuations has a tendency to increase, whereas the range of the potential fluctuations has a tendency to decrease. While, this is not the case here. The light-induced increase in the density of charged defects results from the much more decrease in the range than in the depth.

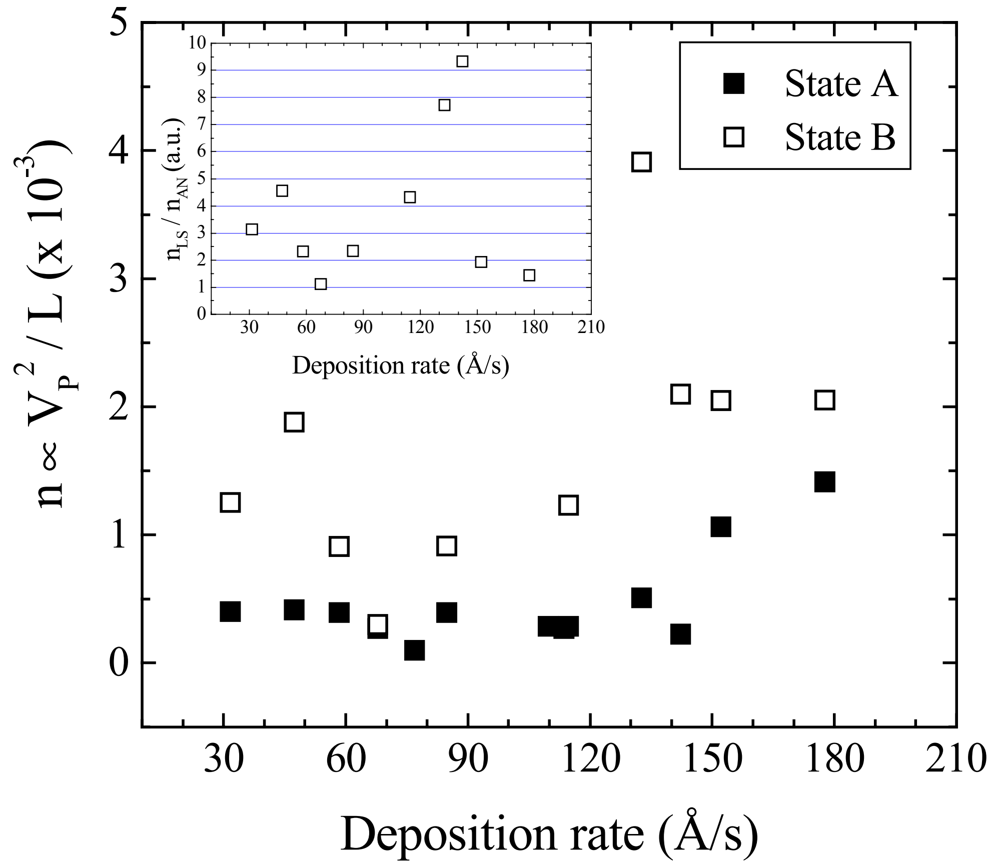

Figure 26. *The light-induced relative change in the charged defect density as a function of deposition rate.*

7. Photoconductive Frequency Mixing Measurements on TCO

We obtained samples of 1% Cd doped HRT, 1% Zn doped HRT and undoped samples from Randy Bohn at the University Toledo to see if we can measure the drift mobility by frequency mixing. We observed a photoconductivity signal at ~5286.5 cm^{-1} employing our Argon laser but we did not observe a mixing signal initially; since it was not clear what the spectral range of the absorption was for these films, we did not employ long integration times. Since that time, Randy Bohn has supplied us with the spectral absorption of these samples, and we will attempt to measure the drift mobility as was suggested by Bolko von Roedern.

References

[1] E.R.Geissinger, R. Braunstein, S.Dong, and R. Martin, J. Appl. Phys. **69**, 1469 (1991).

[2] Y. Tang, R. Braunstein, and B. von Roedern, Appl. Phys. Lett. **63**, 2393 (1992).

[3] Y. Tang, R. Braunstein, B. von Roedern, and F.R. Shapiro, Mat. Res. Soc. Symp. Proc. **297**, 407 (1993).

[4] Y. Tang and R. Braunstein, Appl. Phys. Lett. **66**, 721 (1995).

[5] Y. Tang and R. Braunstein, J. Appl. Phys. **79**, 850 (1996).

[6] Y. Tang, S. Dong, R. Braunstein, and B. von Roedern, Appl. Phys. Lett. **68**, 640 (1996).

[7] S. Reynolds, C. Main, D.P. Webb and M.J. Rose, Mater. Res. Soc., 1999, Vol. 557, p.427-32

[8] D. V. Tsu, B. S. Chao, S. R. Ovshinsky, S. Guha, and J. Yang, Appl. Phys. Lett., **71**, 1317 (1997)

[9] S. Sheng, X. Liao, G. Kong, and H. Han, Appl. Phys. Lett., **73**, 336 (1998)

[10] S. Sheng, X. Liao, Z. Ma, G. Yue, Y. Wan, and G. Kong, submitted for publication to J. App. Phys.

[11] S. Guha, J. Yang, S. Jones, Y. Chen, and D. Williams, Appl. Phys. Lett. **61**,144 (1992)

[12] T. Takagi, R. Hayashi, A. Payne, W. Futako, T. Nishimoto, M. Takai, M. Kondo, and A. Matsuda, Mat. Res. Soc. Symp. Proc. **557,** 105 (1999)

Publications

1-Determination of the gap state density differences in hydrogenated amorphous silicon and Si/Ge

J. Liege, A. Kattwinkel, K. Baerner, G.Sun, S.Dong, R.Braunstein
[Materials Science and Engineering, **A282** 158-163 (2000)]

2-Electronic properties of hydrogenated amorphous silicon-germanium alloys and long-range potential fluctuations

S.R. Sheng, G.S. Sun, J. Liebe, A. Kattwinkel, R. Braunstein, B.P. Nelson, B. von Roedern, and K. Bärner (to be appear in Material Science Engineering A)

REPORT DOCUMENTATION PAGE

Form Approved
OMB NO. 0704-0188

Public reporting burden for this collection of information is estimated to average 1 hour per response, including the time for reviewing instructions, searching existing data sources, gathering and maintaining the data needed, and completing and reviewing the collection of information. Send comments regarding this burden estimate or any other aspect of this collection of information, including suggestions for reducing this burden, to Washington Headquarters Services, Directorate for Information Operations and Reports, 1215 Jefferson Davis Highway, Suite 1204, Arlington, VA 22202-4302, and to the Office of Management and Budget, Paperwork Reduction Project (0704-0188), Washington, DC 20503.

1. AGENCY USE ONLY (Leave blank)	2. REPORT DATE August 2001	3. REPORT TYPE AND DATES COVERED Annual Subcontract Report 19 April 1999 – 20 April 2000

4. TITLE AND SUBTITLE
Photocharge Transport and Recombination Measurements in Amorphous Silicon Films and Solar Cells by Photoconductive Frequency Mixing:
Annual Subcontract Report, 20 April 1999 – 19 April 2000

5. FUNDING NUMBERS
CF: XAK-8-17619-24
PVP15101

6. AUTHOR(S)
R. Braunstein, A. Kattwinkel, and S.R. Sheng

7. PERFORMING ORGANIZATION NAME(S) AND ADDRESS(ES)
University of California
Los Angeles, California

8. PERFORMING ORGANIZATION REPORT NUMBER

9. SPONSORING/MONITORING AGENCY NAME(S) AND ADDRESS(ES)
National Renewable Energy Laboratory
1617 Cole Blvd.
Golden, CO 80401-3393

10. SPONSORING/MONITORING AGENCY REPORT NUMBER
NREL/SR-520-30811

11. SUPPLEMENTARY NOTES
NREL Technical Monitor: Bolko von Roedern

12a. DISTRIBUTION/AVAILABILITY STATEMENT
National Technical Information Service
U.S. Department of Commerce
5285 Port Royal Road
Springfield, VA 22161

12b. DISTRIBUTION CODE

13. ABSTRACT *(Maximum 200 words)* This report describes research focused on improving the individual component cells from which the multijunction devices are fabricated. The Mid-Bandgap and Metastability subteam and the Low-Bandgap subteam have the responsibility to develop appropriate materials for the respective layer of the triple-junction solar cell. To this end, it is necessary to characterize the materials that are prepared for the appropriate layer to optimize the devices and to develop an understanding of the conditions responsible for light-induced degradation so as to develop means to mitigate the degradation. Using the photomixing technique, UCLA was able to determine the mobility and lifetime separately of a number of semiconductor materials. We have established that different kinetics of degradation occur for mobility and lifetime. We have found that the drift mobility is electric-field dependent, and we developed a model for the charge transport through long-range potential fluctuations that enable a determination of the range and the depth of these fluctuations for material in the annealed and light-soaked states. UCLA has continued to provide transport parameters for the Mid-Gap, Metastability, and Low-Band teams. The materials studied were prepared by various deposition techniques.

In phase II of this program, we investigated in detail the charge-transport properties by photomixing of a-Si:H, μc-Si:H and a-SiGe:H alloy films prepared by hot-wire chemical vapor deposition (HWCVD) and plasma-enhanced chemical vapor deposition (PECVD) techniques, particularly under the conditions of high deposition rate and the transition from amorphous to microcrystalline state. Photomixing experiments were initiated to compare intrinsic film properties and device performance, and to study the impact of the changed contact geometry on the results of our photomixing measurements. We also attempted to employ the photomixing technique to measure the drift mobility of the transparent conducting oxide. Following our previous measurements of the transport parameters under hydrostatic pressure, we initiated the hydrostatic pressure dependence of small-angle X-ray scattering measurements to find the origin of the inelastic effect. Time-resolved photo- and thermoelectric effects (TTE) were used to simultaneously determine the thermal diffusivity, carrier lifetime, carrier mobility, and trap-level density in crystalline and amorphous Si (a-Si:H) and Si/Ge (a-Si/Ge:H) samples.

14. SUBJECT TERMS: PV; triple-junction solar cell; light-induced degradation; photomixing measurements; charge-transport properties; hydrostatic pressure; high deposition rate; HWCVD; PECVD;

15. NUMBER OF PAGES

16. PRICE CODE

17. SECURITY CLASSIFICATION OF REPORT	18. SECURITY CLASSIFICATION OF THIS PAGE	19. SECURITY CLASSIFICATION OF ABSTRACT	20. LIMITATION OF ABSTRACT
Unclassified	Unclassified	Unclassified	UL